

## Redox properties of Cu<sub>2</sub>O(100) and (111) surfaces

C. Wang, D. Stacchiola

To be published in "The Journal of Physical Chemistry C"

November 2018

Center for Functional Nanomaterials  
**Brookhaven National Laboratory**

**U.S. Department of Energy**  
USDOE Office of Science (SC), Basic Energy Sciences (BES) (SC-22)

Notice: This manuscript has been authored by employees of Brookhaven Science Associates, LLC under Contract No. DE-SC0012704 with the U.S. Department of Energy. The publisher by accepting the manuscript for publication acknowledges that the United States Government retains a non-exclusive, paid-up, irrevocable, world-wide license to publish or reproduce the published form of this manuscript, or allow others to do so, for United States Government purposes.

## **DISCLAIMER**

This report was prepared as an account of work sponsored by an agency of the United States Government. Neither the United States Government nor any agency thereof, nor any of their employees, nor any of their contractors, subcontractors, or their employees, makes any warranty, express or implied, or assumes any legal liability or responsibility for the accuracy, completeness, or any third party's use or the results of such use of any information, apparatus, product, or process disclosed, or represents that its use would not infringe privately owned rights. Reference herein to any specific commercial product, process, or service by trade name, trademark, manufacturer, or otherwise, does not necessarily constitute or imply its endorsement, recommendation, or favoring by the United States Government or any agency thereof or its contractors or subcontractors. The views and opinions of authors expressed herein do not necessarily state or reflect those of the United States Government or any agency thereof.

# Redox properties of Cu<sub>2</sub>O(100) and (111) surfaces

Chunlei Wang<sup>1</sup>, Heloise Tissot<sup>1</sup>, Carlos Escudero<sup>2</sup>, Virginia Pérez-Dieste<sup>2</sup>, Dario Stacchiola<sup>3</sup>,  
Jonas Weissenrieder<sup>1,\*</sup>

<sup>1</sup> Material Physics, School of Engineering Sciences, KTH Royal Institute of Technology, SE-100 44 Stockholm, Sweden

<sup>2</sup> Alba Synchrotron Light Source, Carrer de la Llum 2-26, 08290-Cerdanyola del Vallès, Barcelona, Spain

<sup>3</sup> Brookhaven National Laboratory, Chemistry Division, P.O. Box 5000, Upton, NY 11973-5000, USA

## Abstract

Intense research efforts are directed towards Cu and Cu<sub>2</sub>O based catalysts as they are viewed as potential replacements for noble metal catalysts. However, applications are complicated by deactivation, e.g. through complete oxidation to CuO. Despite the importance of the redox processes for Cu<sub>2</sub>O catalysts a molecular level understanding of the deactivation process is still lacking. Therefore we study the initial stages of oxidization of well-defined Cu<sub>2</sub>O bulk single crystals of (100) and (111) termination by means of synchrotron radiation X-ray photoemission spectroscopy (XPS) and scanning tunneling microscopy (STM). Exposure of the (100) surface to 1 mbar O<sub>2</sub> at 25 °C result in formation of a 1.0 monolayers (ML) CuO surface oxide. The surface is also covered by 0.7 ML OH groups from unavoidable trace moisture in reaction gas. In contrast, neither hydroxylation nor oxidation was observed on the (111) surface under similar exposure conditions. On (111) the formation of CuO did only commence after annealing to ~400 °C in 1 mbar O<sub>2</sub>, highlighting the different character of the two surfaces. Annealing of the (100) surface, under ultrahigh vacuum conditions, to temperatures up to ~225 °C resulted in removal of the OH groups (0.46 ML decrease) at a rate similar to a detected increase in CuO coverage (0.45 ML increase), suggesting the reaction path  $2\text{OH}_{\text{adsorbed}} + \text{Cu}_2\text{O}_{\text{solid}} \rightarrow \text{H}_2\text{O}_{\text{gas}} + 2\text{CuO}_{\text{solid}}$ . STM was used to correlate the observed changes in surface chemistry with surface morphology, confirming the surface hydroxylation and CuO formation. The STM analysis showed dramatic changes in surface morphology demonstrating a high mobility of the active species under reaction conditions.

Keywords: Cu<sub>2</sub>O (100) and (111), Near-ambient pressure, PES and STM, oxidation and reduction.

\* Corresponding author: [jonas@kth.se](mailto:jonas@kth.se)

## 1. Introduction

Copper and copper oxide based catalysts show promise for application in several catalytic reactions, such as CO oxidation,<sup>1-4</sup> the water gas shift reaction,<sup>5-6</sup> selective oxidation of propylene,<sup>7-8</sup> methanol dehydrogenation<sup>9-10</sup>, NO reduction<sup>11</sup> and photocatalytic water splitting.<sup>12-13</sup> Efficient noble metal based catalysts are available for several of these reactions, but scarcity and rising costs make substitution by cheaper and more abundant materials highly attractive.<sup>14-16</sup> Since copper is both relatively affordable and abundant it constitutes a prime candidate for future replacement of noble metal catalysts.<sup>17-18</sup> <sup>19</sup> However, the deactivation of copper based catalyst through oxidation has hindered its development. Under ambient atmosphere the oxidation of copper proceeds through an initial formation of a thin film of cuprous oxide (Cu<sub>2</sub>O). Upon further exposure copper will eventually become fully oxidized (CuO).<sup>20-21</sup> The formation of CuO results in loss of catalytically active Cu<sup>+</sup> centers and therefore is determining the oxidation and reduction properties of cuprous oxide critical for the understand the deactivation processes of copper catalyst.

The application of single crystal model systems for studies using a combination of surface sensitive techniques, such as X-ray photoelectron spectroscopy (XPS), low-energy electron diffraction (LEED), and scanning tunneling microscopy (STM), have an impressive track record for determining the relationship between atomic structure and reactivity of catalytic surfaces.<sup>22-23</sup> For Cu<sub>2</sub>O, the interaction of single crystals with reaction gases has been the focus of several studies resulting in an understanding, at the atomic level, of how the surface is modified by adsorbates.<sup>24-26</sup> Under ambient conditions the oxidation and corrosion of copper surfaces is influenced by gas phase stimulators that accelerate the process, including H<sub>2</sub>O,<sup>27-29</sup> CO<sub>2</sub>,<sup>30</sup> CO,<sup>31-32</sup> H<sub>2</sub>,<sup>33</sup> O<sub>2</sub>,<sup>24, 34-35</sup> H<sub>2</sub>S,<sup>36</sup> SO<sub>2</sub>,<sup>27</sup> NO<sub>x</sub>,<sup>37</sup> and organic molecules.<sup>10, 38</sup> However, O<sub>2</sub> and H<sub>2</sub>O are the most important for the fundamental oxidation process. In pioneering studies, Schulz et al. exposed Cu<sub>2</sub>O(100) surfaces to high doses of O<sub>2</sub> and showed that the reported  $(3\sqrt{2} \times \sqrt{2})R45^\circ$  reconstruction of the ultrahigh vacuum (UHV) prepared surface was modified to a  $(1 \times 1)$  periodicity. Annealing the surface to above 227 °C restored the surface to its original reconstructed state.<sup>24</sup> Another study by Bowker et al. showed formation of CuO on both thick films and bulk Cu<sub>2</sub>O by annealing at 600 °C in  $1 \times 10^{-4}$  mbar O<sub>2</sub>.<sup>35</sup> Further, first principle simulations have determined dissociative adsorption of O<sub>2</sub> as favorable over molecular

adsorption on several  $\text{Cu}_2\text{O}$  surfaces,<sup>39-40</sup> and the presence of oxygen vacancies on  $\text{Cu}_2\text{O}(111)$  enhance the activity for  $\text{O}_2$  dissociation.<sup>34</sup>

Under ambient conditions water is a ubiquitous reactant both as humidity in the gas phase and as thin films covering all exposed surfaces. The presence of  $\text{H}_2\text{O}$  greatly influences surface chemistry and is regarded as the most important corrosion stimulant for the corrosion of copper.<sup>41-42</sup> Cox and Schulz reported in a study of single crystal  $\text{Cu}_2\text{O}$  that  $\text{H}_2\text{O}$  exposure at 110 K resulted in both dissociative and molecular adsorption, while at 300 K only dissociative adsorption was observed. In temperature programmed desorption (TPD) analysis  $\text{H}_2\text{O}$  was exclusively detected as desorption product,<sup>29</sup> which is consistent with water desorption studies on other oxide systems.<sup>43-46</sup> Nygren et al. investigated  $\text{H}_2\text{O}$  adsorption on the  $\text{Cu}_2\text{O}(100)$  surface and found that dissociative adsorption is energetically favorable.<sup>47</sup> Deng et al. prepared  $\text{Cu}_2\text{O}$  thin films through in situ oxidation of a copper foil and suggested the importance of oxygen vacancies and other surface defects for promotion of water dissociation.<sup>28</sup> Stenlid et al. studied the  $\text{H}_2\text{O}$  interaction with well-defined  $\text{Cu}_2\text{O}(100)$  surfaces by a combination of DFT and XPS and determined adsorption sites and stability of different coverage of hydrogen, hydroxyl groups, and water.<sup>48</sup> R. Zhang et al. showed, through DFT simulations, dissociative adsorption of water on oxygen pre-covered  $\text{Cu}_2\text{O}(111)$  surfaces.<sup>49</sup> Although, several studies have focused on the water adsorption process on single crystal  $\text{Cu}_2\text{O}$  surfaces, the corresponding desorption process is not as well understood.

In order to determine the influence of surface termination and the processes involved in the initial surface oxidation of  $\text{Cu}_2\text{O}$ , single crystals of (100) and (111) terminations were investigated by means of atomic resolution STM and near ambient pressure X-ray photoemission spectroscopy (NAPXPS). The  $\text{O}_2$  exposures covered pressures from  $1 \times 10^{-3}$  mbar to 10 mbar.  $\text{CuO}$  formation and hydroxylation was observed on the  $\text{Cu}_2\text{O}(100)$  surface already at room temperature, while  $\text{Cu}_2\text{O}(111)$  required annealing to  $400^\circ\text{C}$  in 1 mbar  $\text{O}_2$  before  $\text{CuO}$  formation commence. The oxidized surfaces were subsequently reduced by annealing under UHV conditions and the surface composition was followed as a function of temperature. In parallel experiments using STM the surface structure and morphology was investigated under similar exposure conditions. Together the analysis provides a comprehensive description of changes in surface morphology and the oxidation/reduction reactions taking place on  $\text{Cu}_2\text{O}$  surfaces.

## 2. Experimental

The Cu<sub>2</sub>O (100) and Cu<sub>2</sub>O (111) single crystals used in the present research were purchased from Surface Preparation Laboratory, the Netherlands. Clean and well-ordered surfaces were prepared by cycles of argon ion sputtering (0.5 kV) and annealing in oxygen at  $2 \times 10^{-6}$  mbar followed by annealing in UHV. Both the O<sub>2</sub> and UHV annealing was performed at 550-650 °C for a duration of at least 10 min. The preparation procedure resulted in well-ordered (3,0;1,1) and  $(\sqrt{3} \times \sqrt{3})R30^\circ$  reconstructions on the (100) and (111) surfaces, respectively. The cleanliness and surface order was confirmed by LEED and STM directly, or by LEED and XPS wide scans and at common contamination regions, e.g. potassium and carbon.

The surface of Cu<sub>2</sub>O(100) was analyzed using the NAPXPS endstation at beamline 24 (CIRCE) at ALBA.<sup>50</sup> The photon energy range at CIRCE is 100 – 2000 eV and the end station is equipped with a Phoibos NAP 150 electron energy analyzer. Sample preparation was performed in a preparation chamber in direct connection with the analysis chamber. All the gas doing was performed using high-precision leak valves. The Cu<sub>2</sub>O(111) surface was analyzed using the NAPXPS endstation of the HIPPIE beamline at the MAX IV laboratory in Lund, Sweden. The endstation consists of an analysis chamber equipped with a Scienta-Omicron HiPP-3 electron energy analyzer. An ambient pressure cell (AP Cell) was docked to the analyzer for the near ambient pressure experiments. All gas was dosed using a computer controlled gas handling system. Sample preparation was performed in a separate preparation chamber in connection with the analysis chamber.

The STM was carried out using an Omicron VT-STM operated in constant current imaging mode with electrochemically etched tungsten tips. The STM-chamber is attached to a preparation chamber equipped with an argon ion sputter gun, leak-valves, and a LEED-apparatus. A high-pressure reaction cell mounted on the preparation chamber was used for exposure to mbar pressures of oxygen gas. The sample manipulation system allows for direct transfer between the high pressure cell, the preparation, and the STM chambers.

## 3. Results

Carefully prepared crystal surfaces exhibiting sharp a (3,0;1,1) LEED pattern for Cu<sub>2</sub>O(100) and a similarly sharp  $(\sqrt{3} \times \sqrt{3})R30^\circ$  pattern for Cu<sub>2</sub>O(111) were positioned in position for NAPXPS

analysis.<sup>10, 25</sup> Figure 1 show in situ O 1s spectra from the two terminations under A) increasing O<sub>2</sub> pressure at 25 °C for Cu<sub>2</sub>O(100) and B) increasing pressure and temperature for Cu<sub>2</sub>O(111). The clean surface of the Cu<sub>2</sub>O must be described with a minimum of two components. The main peak for Cu<sub>2</sub>O(100) is positioned at a binding energy of 530.3 eV. This peak is assigned to oxygen atoms in bulk lattice positions in the Cu<sub>2</sub>O crystal.<sup>51</sup> A low binding energy shoulder to the bulk oxygen component is evident at 529.5 eV. This peak has previously been assigned to under-coordinated surface oxygen atoms taking part in the (3,0;1,1) reconstruction.<sup>48</sup> The position of the main peak of Cu<sub>2</sub>O(111) is located at 530.1 eV and the shoulder attributed to under-coordinated oxygen atoms at the surface is at a binding energy of 529.2 eV.<sup>27</sup> Figure 1 includes spectra collected in the oxygen pressure range from  $1 \times 10^{-3}$  to 1 mbar O<sub>2</sub>. For the Cu<sub>2</sub>O(100) surface, Figure 1A, an additional peak on the high binding energy side of the bulk component emerge already at  $10^{-3}$  mbar O<sub>2</sub>. The component, positioned at 531.4 eV, is assigned to formation of hydroxyl groups on the surface. The rapid hydroxylation from trace levels of water in the reaction gas reflects the high affinity of the (100) surface to dissociative H<sub>2</sub>O adsorption.<sup>28-29, 47, 52</sup> Simultaneous to the hydroxyl formation, the peak on the low binding energy side of the component assigned to oxygen atoms in bulk lattice positions is shifted to about 529.3 eV. This shift reflects the formation of a surface oxide of CuO composition. CuO exhibit a similar binding energy position as the under-coordinated oxygen atoms.<sup>35, 48, 51</sup> The coverage of the different components was estimated using the photoelectron mean free path and the intensity of the fitted components of the O 1s (Figure S2). The resulting coverage was normalized to the number of copper sites on the Cu<sub>2</sub>O surface.<sup>27, 48</sup> As shown in Figure 2, with increasing O<sub>2</sub> pressure follows an increase in coverage of both CuO and OH on the Cu<sub>2</sub>O (100) surface.

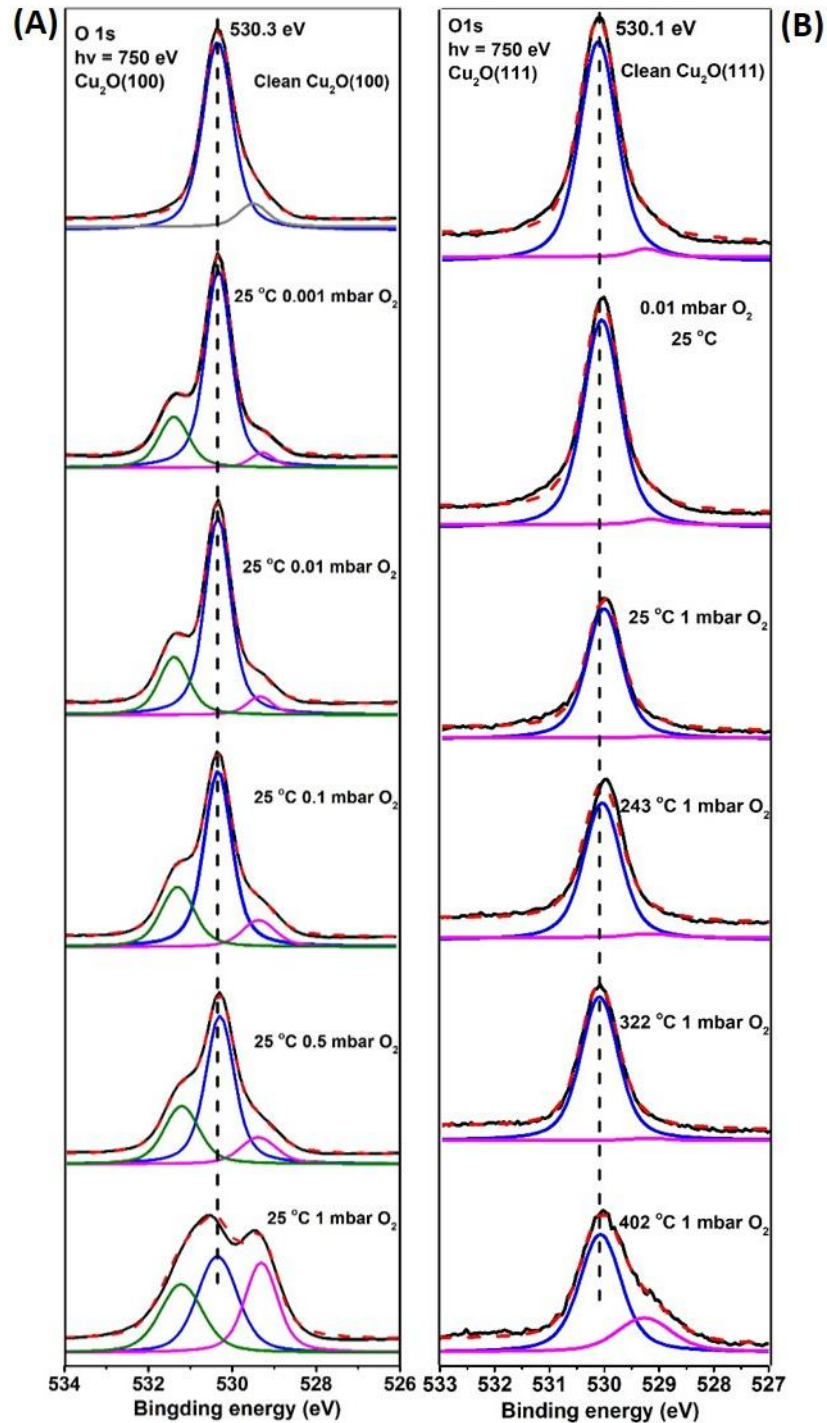


**Figure 1:** XPS spectra from the O 1s core level under near ambient pressures of O<sub>2</sub>. (A) Cu<sub>2</sub>O(100) isotherm experiment at 25 °C with increasing O<sub>2</sub> pressure from  $1 \times 10^{-3}$  to 1 mbar (B) Cu<sub>2</sub>O(111) at an increasing pressure and temperature. Red dashed lines are results of the fitting and the black lines experimental data. The clean surface was collected before exposing to O<sub>2</sub>. All spectra were collected at a photon energy of 750 eV.

In the pressure range from  $1 \times 10^{-3}$  to  $1 \times 10^{-2}$  mbar  $O_2$  only a modest increase in surface CuO is observed, with surface coverages around 0.16 ML. However, a dramatic increase in CuO concentration was observed when increasing the  $O_2$  pressure further. At 0.1 mbar the coverage of CuO increased to 0.3 ML and at 1 mbar  $O_2$  the CuO coverage reached 0.98 ML. We also observe an increase in coverage of interface hydroxyls with increasing  $O_2$  pressure. Thus simultaneous oxidation and hydroxylation processes occur on the  $Cu_2O(100)$  surface.

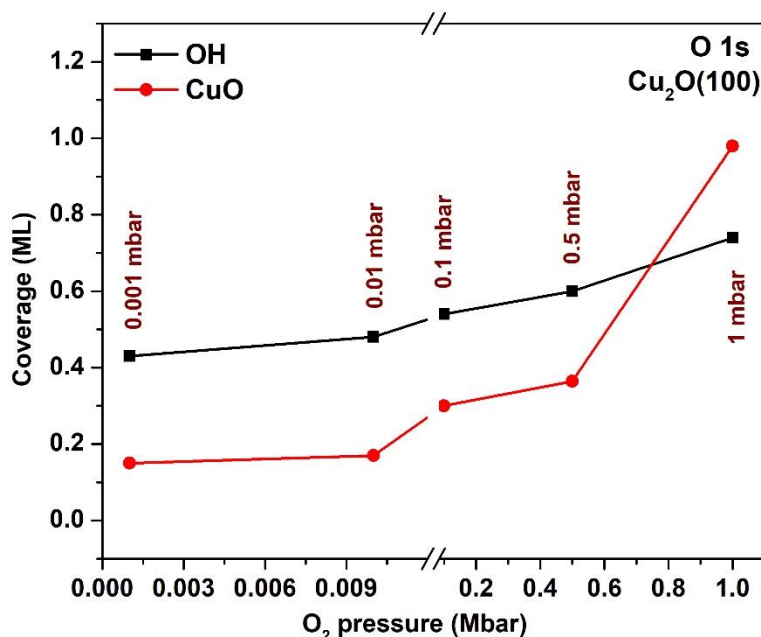


**Figure 2.** Coverage of surface OH and CuO on  $Cu_2O(100)$  as a function of oxygen partial pressure.

In contrast to the results shown for the (100) surface, no clear oxidation or hydroxylation was observed under similar exposure conditions for the  $Cu_2O(111)$  surface (Figure 1B). Not even under 1 mbar  $O_2$ . In order to initiate the CuO formation, the sample was therefore annealed to  $\sim 400$  °C in 1 mbar  $O_2$  when a distinct CuO surface oxide component appeared at the binding energy position 529.2 eV. Prior to CuO formation no apparent hydroxylation was observed on the surface, reflecting the strikingly different character of the two  $Cu_2O$  terminations. A slight shift in position, towards lower binding energy, of the main component assigned to oxygen atoms in bulk lattice positions was observed at 25 °C and elevated pressures of  $O_2$ . The chemical shift between the bulk oxygen lattice peak and the under-coordinated sites remained constant at around 0.91 eV (see Table S1). We interpret the shift of the spectrum as due to adsorbate

induced band bending. In line with this interpretation is the observation that the relative intensity of the under coordinated O 1s component at 1 mbar O<sub>2</sub> decreased to approximately 1/3 of the corresponding intensity on the clean surface. This decrease indicates adsorbate interaction with surface sites, tentatively low coverage of adsorbed oxygen or OH. After annealing to ~325 °C the binding energy positions in the O 1s spectrum was restored to the position of the clean surface, indicating that the adsorbates had desorbed from the surface at this temperature. Additional O 1s results are shown in Figure S1.

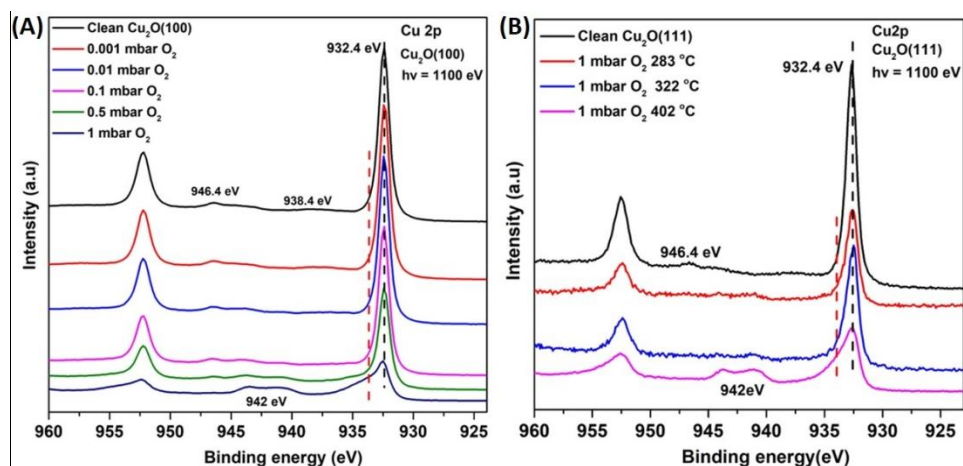


**Figure 3.** Cu 2p photoemission spectra of (A) Cu<sub>2</sub>O(100) under different near-ambient oxygen pressures and (B) Cu<sub>2</sub>O (111) under 1 mbar O<sub>2</sub> at an increasing high temperature. All spectra were collected at a photon energy of 1100 eV.

To corroborate the analysis from the O 1s we also studied the Cu 2p core level under the same conditions (Figure 3). The clean Cu<sub>2</sub>O surface exhibit a Cu 2p<sub>3/2</sub> line position at 932.4 eV, corresponding to Cu<sup>+</sup> sites in the lattice.<sup>35, 51</sup> During the initial oxygen exposure of the (100) surface the Cu 2p core level showed no distinct signs of oxidation, however when the oxygen pressure was increased to 0.1 mbar a shoulder appeared on the high binding energy side of the 2p<sub>3/2</sub> peak. The position of the shoulder is indicated by the red dashed line in Figure 3A at a binding energy position in good agreement with that of CuO at 933.6 eV.<sup>35</sup> Simultaneous to the appearance of the CuO assigned shoulder, we observe peaks at positions corresponding to the shake-up of Cu<sup>2+</sup> at around 942 eV. In Figure 3B, the corresponding spectra from the Cu<sub>2</sub>O(111) surface is shown. Under 1 mbar O<sub>2</sub> the oxidation proceeds only slowly until a temperature of ~400 °C is reached, when rapid formation of CuO is observed (in agreement with the O 1s

spectra). From the core level analysis under near ambient pressures of oxygen we can conclude that the  $\text{Cu}_2\text{O}(100)$  surface is rapidly oxidized and hydroxylated already at room temperature while at the  $\text{Cu}_2\text{O}(111)$   $\text{CuO}$  formation require annealing to approximately  $400\text{ }^\circ\text{C}$  and if hydroxylation occurs it is only at very low levels.

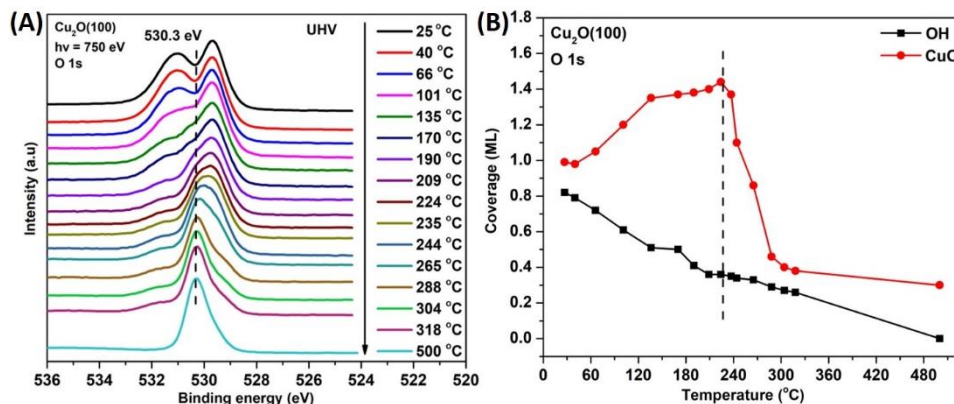


**Figure 4.** UHV annealing of the at 1 mbar  $\text{O}_2$  pre-oxidized  $\text{Cu}_2\text{O}(100)$  surface. (A) O 1s spectra collected during the annealing process show desorption of hydroxyl groups and the reduction of the  $\text{CuO}$  surface oxide; (B) Coverages of OH and  $\text{CuO}$  on the  $\text{Cu}_2\text{O}(100)$  surface as a function of temperature.

Following the exposure of the  $\text{Cu}_2\text{O}(100)$  surface to 1 mbar  $\text{O}_2$ , the analysis chamber was evacuated and photoemission of spectra was collected in UHV as a function of temperature (Figure 4A). The hydroxyl groups were gradually removed from the surface as the temperature increased from  $25\text{ }^\circ\text{C}$  to  $500\text{ }^\circ\text{C}$ . In a quantitative analysis, all spectra collected was deconvoluted into its components and the relative peak areas as percentage of the total O 1s intensity is shown in Figures S3 and S4. In Figure 4B the peak intensities were calculated into surface coverage by using the mean free path of the photoelectrons. For reasons of clarity the analysis of the temperature resolved results are divided into two parts, below and above  $\sim 225\text{ }^\circ\text{C}$  (as indicated by the vertical black dashed line in figure 4B). Below  $\sim 225\text{ }^\circ\text{C}$ , an approximately linear decrease in OH coverage is observed, from 0.82 ML at room temperature to 0.36 ML at  $\sim 225\text{ }^\circ\text{C}$ . Simultaneous to the decrease in OH, the coverage of  $\text{CuO}$  increase from 0.99 ML to 1.44 ML. The decrease in OH coverage (0.46 ML decrease) is close to the increase in coverage of surface  $\text{CuO}$  (0.45 ML increase). After room temperature exposure to the reaction gas, the  $\text{Cu}_2\text{O}(100)$

surface exhibit a high hydroxyl coverage ( $> 0.5$  ML) that has previously been shown to crowd out the hydrogen atoms from the dissociatively adsorbed  $\text{H}_2\text{O}$ , resulting in recombinative desorption of  $\text{H}_2$  before commencing the heat treatment.<sup>48</sup> Taken together, the results indicate that OH desorb from the surface through the reaction  $2\text{OH}_{\text{surface}} + \text{Cu}_2\text{O}_{\text{solid}} \rightarrow \text{H}_2\text{O}_{\text{gas}} + 2\text{CuO}_{\text{solid}}$ . The oxygen atom from the two recombining hydroxyl groups that does not leave the surface as  $\text{H}_2\text{O}$  reacts with the  $\text{Cu}_2\text{O}$  substrate to form a surface layer of  $\text{CuO}$ . At temperatures above  $\sim 225$  °C, we observe a sharp decrease in  $\text{CuO}$  coverage with increasing temperature. This can be explained by a reduction of  $\text{CuO}$  at a combined elevated temperature and low oxygen partial pressure and is consistent with other reports in the literature.<sup>24, 35</sup>

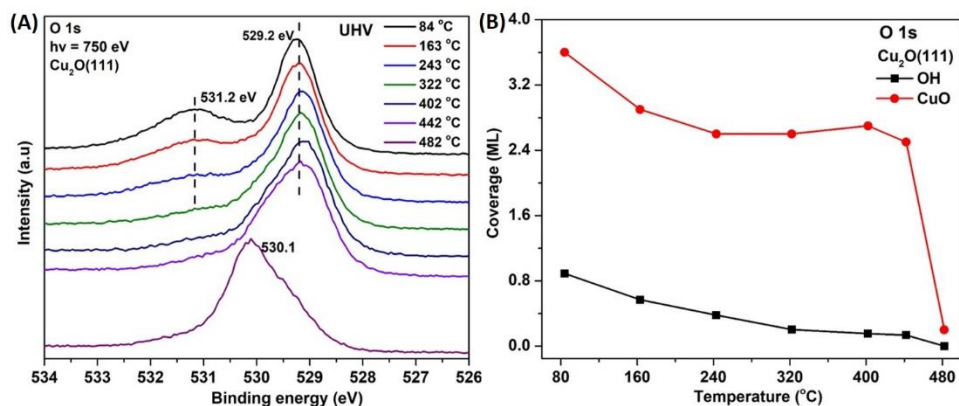


**Figure 5.** UHV annealing of the  $\text{Cu}_2\text{O}$  (111) surface following oxidation in at 1 mbar  $\text{O}_2$  and  $\sim 400$  °C. (A) O 1s spectra collected during the annealing process show desorption of hydroxyl groups and reduction of the  $\text{CuO}$  surface oxide; (B) Coverages of OH and  $\text{CuO}$  on the  $\text{Cu}_2\text{O}$ (111) surface as a function of temperature.

We continue to describe the reduction of the oxidized  $\text{Cu}_2\text{O}$ (111) surface. After the formation of a  $\text{CuO}$  surface oxide at 1 mbar  $\text{O}_2$  and  $\sim 400$  °C, the sample temperature was slowly reduced under 1 mbar  $\text{O}_2$ . At 25 °C the AP Cell was evacuated and XPS spectra was collected in UHV as a function of temperature. The O 1s spectra in Figure 5A show that at 84 °C the (111) surface exhibit a close to completely oxidized surface with the main peak at a 529.2 eV binding energy, corresponding to the peak position of  $\text{CuO}$ .<sup>35, 51</sup> In the same spectrum we also observe a peak located at higher binding energy, 531.2 eV, which is assigned to hydroxyl groups. The presence of hydroxyl groups after oxidation show that OH groups will more readily be formed on the  $\text{CuO}$

surface oxide than on the clean Cu<sub>2</sub>O(111) surface where no OH groups were detected. The OH groups are completely removed after annealing to 482 °C and the surface is mostly restored Cu<sub>2</sub>O(111), but some traces of CuO remains. In Figure 5B we show the coverage of CuO and OH as a function of temperature, as determined using the photoelectron mean free path. In contrast to the reduction of oxidized Cu<sub>2</sub>O(100) both OH and CuO coverage decrease steadily with temperature up to approximately 250 °C. At this temperature the coverage of CuO has decreased by approximately 1 ML and the coverage of OH by 0.5 ML. In the temperature range between approximately 250 °C and 400 °C the dehydration slows down as a function of temperature and we observe a slight increase in CuO coverage. Tentatively the same reaction as reported for Cu<sub>2</sub>O(100),  $2\text{OH}_{\text{surface}} + \text{Cu}_2\text{O}_{\text{solid}} \rightarrow \text{H}_2\text{O}_{\text{gas}} + 2\text{CuO}_{\text{solid}}$ , may occur in this temperature range. Close to 400 °C the surface is almost completely dehydrated and a rapid reduction of CuO commence. The corresponding Cu 2p spectra (Figure S7) corroborate the analysis from the O 1s.

STM was used to study changes in atomic structure and morphology taking place on the Cu<sub>2</sub>O surfaces during the redox processes. Specifically the (100) surface was exposed to O<sub>2</sub> at similar pressure and temperature as in the APXPS study to correlate changes in chemical state with surface morphology and atomic structure. Oxidation under near ambient O<sub>2</sub> pressures was conducted in an ambient pressure cell in direct connection with the STM analysis chamber.

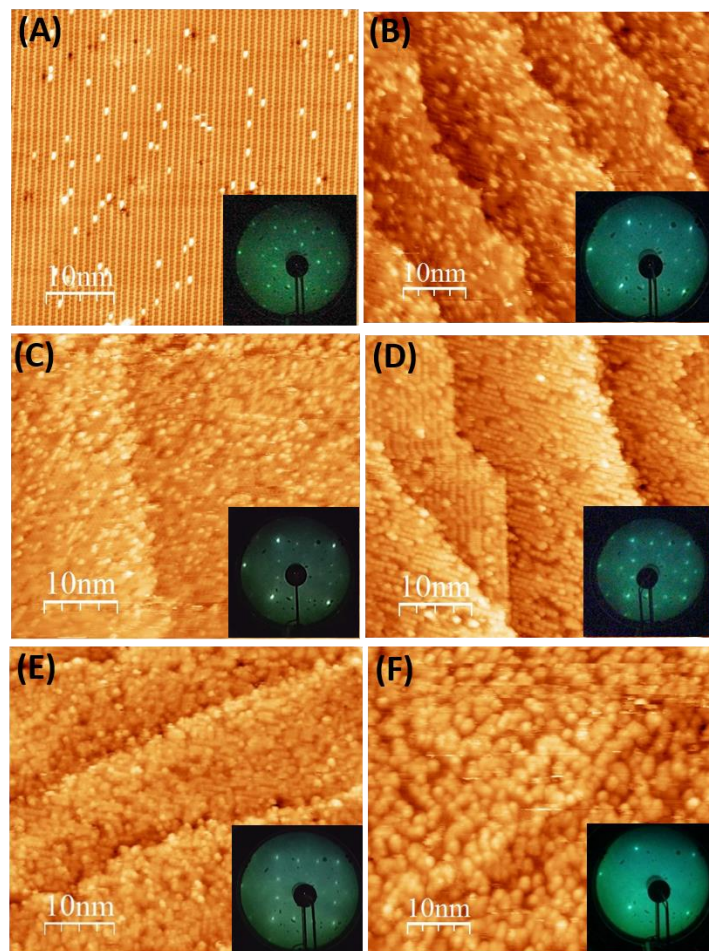


**Figure 6.** Selected STM images of the  $\text{Cu}_2\text{O}(100)$  surfaces after different oxidation steps at near-ambient pressures and 25 °C. (A) the clean (100) surface as prepared in UHV (STM scanning parameters: 2.2 V, 0.18 nA); (B) After 2 min oxidation at  $2 \times 10^{-3}$  mbar  $\text{O}_2$  (2.2 V, 0.14 nA); (C) 1 min oxidation at  $1 \times 10^{-2}$  mbar  $\text{O}_2$  (2.6 V 0.19 nA); (D) 1 min oxidation at 0.1 mbar  $\text{O}_2$  (2.2 V, 0.12 nA); (E) 2 min oxidation at 1 mbar  $\text{O}_2$  (2.1 V, 0.14 nA); (F) 2 min oxidation at 10 mbar  $\text{O}_2$  (1.8 V, 0.1 nA). Inserts: LEED patterns from respective surface collected at 25 eV.

Figure 6 shows how exposure of oxygen gas at increasing pressure influence the surface structure and morphology, as probed by STM and LEED, of the clean (3,0;1,1) reconstructed  $\text{Cu}_2\text{O}(100)$  surface.<sup>25</sup> Exposures up to  $10^{-2}$  mbar  $\text{O}_2$  (Figure 6B at  $2 \times 10^{-3}$  mbar and 6C at  $10^{-2}$  mbar) results in decreased intensity and blurring of the LEED spots associated with the surface reconstruction. With increasing dose an increasing coverage of protrusion is observed with STM. In the areas between the protrusions the characteristic rows of the clean surface can still be observed. Taken together, the XPS and STM results suggests that the oxidation of the surface is only proceeding slowly at these oxygen pressures and the protrusions are probably dominated the

formation of surface OH groups from trace water in the reaction gas dissociating on the surface. At further increased pressures (Figure 6 D at 0.1 mbar), the surface order increase. The ordering is observed both in LEED, as sharper spots, and in STM that show a surface with protrusions aligned in the principal directions of the reconstructed substrate. Approximately one protrusion per (3,0;1,1) unit cell is detected and in contrast to the clean reconstructed surface the rows of protrusions are often discontinuous and bent. The recovery of the LEED pattern and relatively well-ordered rows in STM pictures indicate that the OH groups adsorb in sites with the same periodicity of the (3,0;1,1) surface with a saturation coverage close to 1 OH group per unit cell. At even higher oxygen gas pressures the surface order decrease. Figure 6E show a surface after 1 mbar O<sub>2</sub> 2 min, where the rows of protrusion begin to break up and formation of additional layers of protrusions is evident (additional STM images can be found in Figure S8). After 10 mbar O<sub>2</sub> exposure, the surface is entirely covered by large protrusions suggesting formation of a disordered and hydroxylated surface oxide. The corresponding LEED pattern exhibit the (1×1) periodicity of the bulk Cu<sub>2</sub>O with a high background. The results from STM are consistent with the conclusions from XPS and show that the oxidation of the Cu<sub>2</sub>O(100) proceeds through an initial hydroxylation at low oxygen partial pressures (< 0.1 mbar) followed by formation of a hydroxylated CuO at around 1 mbar O<sub>2</sub> pressure.

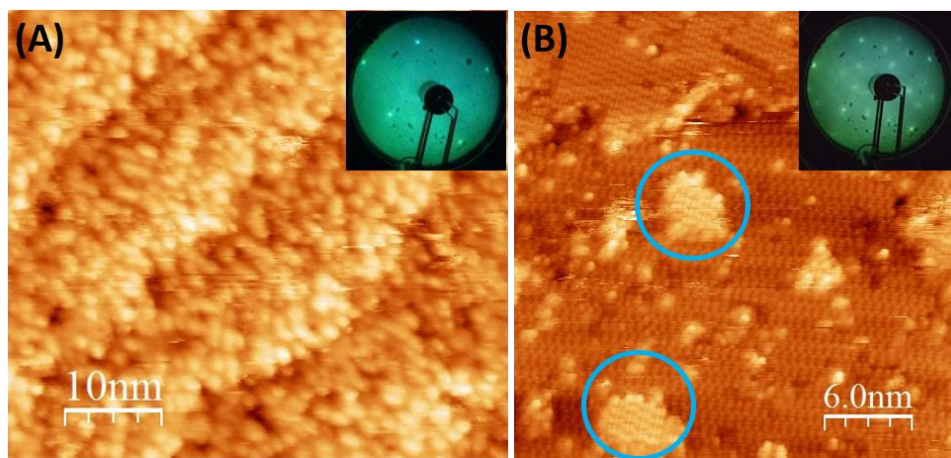


**Figure 7.** STM images after UHV annealing of a Cu<sub>2</sub>O(100) surface pre-oxidized at 10 mbar O<sub>2</sub>. (A) Annealing to 220 °C for 3min, 2.3 V and 0.15 nA; (B) Annealing to 280 °C for 3 min, 2.5 V and 0.12 nA.

After exposure to 10 mbar O<sub>2</sub> the (100) surface was annealed under ultra-high vacuum conditions to investigate the reduction process of the surface oxide. Figure 7A show the surface after an initial annealing step to 220 °C. The LEED pattern still exhibits a (1×1) periodicity with only minor changes in background compared to the, at room temperature, oxidized sample. In STM the surface also resembles the oxidized surface. According to the XPS analysis presented above, a large fraction of the OH groups is removed from the surface through H<sub>2</sub>O desorption and oxygen atoms remaining at the surface form additional CuO. The STM results show that the oxidation of the Cu<sub>2</sub>O(100) surface predominantly proceeds through formation of CuO particles and no ordered CuO surface oxide is formed under the present reaction conditions. At increasing annealing temperatures (Figure 7B, 280 °C), the LEED show a recovery of the reconstructed (3, 0; 1, 1) surface, although the diffraction spots are not quite as intense and sharp as for the UHV prepared clean surface. STM confirms the recovery of the (3, 0; 1, 1) surface, thus annealing in UHV can reduce the formed CuO during oxidation and restore the Cu<sub>2</sub>O(100) surface, in good agreement with the XPS results for the UHV reduction. The STM further reveal details on the dynamics of the surface morphology during reduction. Figure 7B show the formation of numerous Cu<sub>2</sub>O islands on the (100) terraces, blue circles (additional STM images are shown in figure S9). The formation of ad-island indicates high mobility of the surface atoms taking place in the redox reaction process.

#### 4. Discussion

The redox properties of well-characterized Cu<sub>2</sub>O(100) and (111) surfaces was studied by means of LEED, STM, and in-situ XPS. Hydroxylation, from inevitable trace water vapor in the reaction gas, proved to play an important role in the reactions over the (100) surface, both in the initial oxidation process as well as during reducing conditions. The Cu<sub>2</sub>O(100) surface become hydroxylated, by trace impurities in the reaction gas, before significant CuO formation commence. Monolayer coverages of CuO is formed on Cu<sub>2</sub>O(100) at mbar O<sub>2</sub> pressures and room temperature. The CuO formation was accompanied by a an increase in OH coverage, tentatively due to the increased surface area of the CuO as compared to the smooth Cu<sub>2</sub>O(100) surface. Cu<sub>2</sub>O(111) exhibit strikingly different oxidation properties in comparison to the (100) surface. The Cu<sub>2</sub>O(111) surface do not show any significant CuO or hydroxyl formation during exposure to near-ambient oxygen pressures at up to 1 mbar O<sub>2</sub> and room temperature. CuO

formation commence only after increasing the surface temperature to  $\sim 400$  °C at 1 mbar  $O_2$ . After CuO have been formed on the surface and the temperature is reduced to below 100 °C, still under  $O_2$  ambient, hydroxylation of the surface is observed. This demonstrates the affinity for dissociative  $H_2O$  adsorption on the CuO.

Subsequent to the oxidation process the samples were annealed under reducing UHV conditions to deduce the mechanisms of the reduction process. Annealing of  $Cu_2O(100)$  at temperatures up to  $\sim 225$  °C showed an increase in CuO coverage (0.45 ML increase) correlated with a decrease in OH coverage (0.46 ML decrease) indicative of the reaction path:  $2OH + Cu_2O \rightarrow H_2O + 2CuO$ . The recombinative desorption of two OH groups leaves an oxygen atom on the surface that bind to a substrate  $Cu_2O$  unit resulting in the formation of two CuO units at the surface. At temperatures exceeding  $\sim 225$  °C the CuO reduction commence and the reduction is almost complete at  $\sim 300$  °C when the (100) surface is restored to its as prepared (3, 0; 1, 1) reconstruction. The reduction of the oxidized  $Cu_2O(111)$  follow a different rout than the reduction of the oxidized  $Cu_2O(100)$ . The surface OH groups and CuO simultaneously decrease in the temperature range below  $\sim 250$  °C. We observe no evidence of surface atomic oxygen, from recombinative desorption of hydroxyl groups, forming bonds with the  $Cu_2O$  substrate. This indicates that both  $O_2$  and  $H_2O$  desorption pathways are likely to be beneficial. The full reduction of CuO is observed at more than 100 °C higher temperature than on the oxidized (100) surface. This is an indication of that, once formed, the CuO phase is stabilized on the (111) facet.

## 5. Conclusions

In the present work we employ *in-situ* XPS and STM to study the redox properties of two facets of  $Cu_2O$ , the (100) and the (111) surfaces, under near-ambient oxygen pressures. The  $Cu_2O(100)$  readily hydroxylates by trace impurities in the reaction gas and complete oxidation to CuO occur already at room temperature. For  $Cu_2O(111)$ , hydroxylation is not detected on the clean surface and CuO formation only occur after oxidation at  $\sim 400$  °C in 1 mbar  $O_2$ . After CuO is formed, the surface readily hydroxylate at temperatures below 100 °C. These results demonstrate the importance in considering the atomic structure of the terminating surfaces when studying the oxidation and hydroxylation properties.

In the reduction of the hydroxylated CuO phase formed on Cu<sub>2</sub>O(100) we observe a gradual removal of hydroxyl groups below 250 °C. The removal of OH groups is directly coupled to additional formation of CuO at the surface through bonding of residual atomic oxygen from the recombinative H<sub>2</sub>O desorption process with the substrate. The result shows the importance of including corrosion stimulants such as H<sub>2</sub>O, which is present under realistic reaction conditions, in the analysis. Above 250 °C a rapid reduction of CuO is observed resulting in formation of a (3, 0; 1, 1) reconstructed Cu<sub>2</sub>O(100) at approximately 300 °C. For the reduction of the oxidized Cu<sub>2</sub>O(111) surface we do not observe OH driven CuO formation. Instead both OH and CuO coverage decrease simultaneously, indicating that both O<sub>2</sub> and H<sub>2</sub>O desorption pathways are favorable processes. Complete reduction of CuO is only observed close to 500 °C, more than 100 °C higher temperature than on the oxidized (100) surface. This is an indication of that, once formed, the CuO phase is stabilized on the (111) facet.

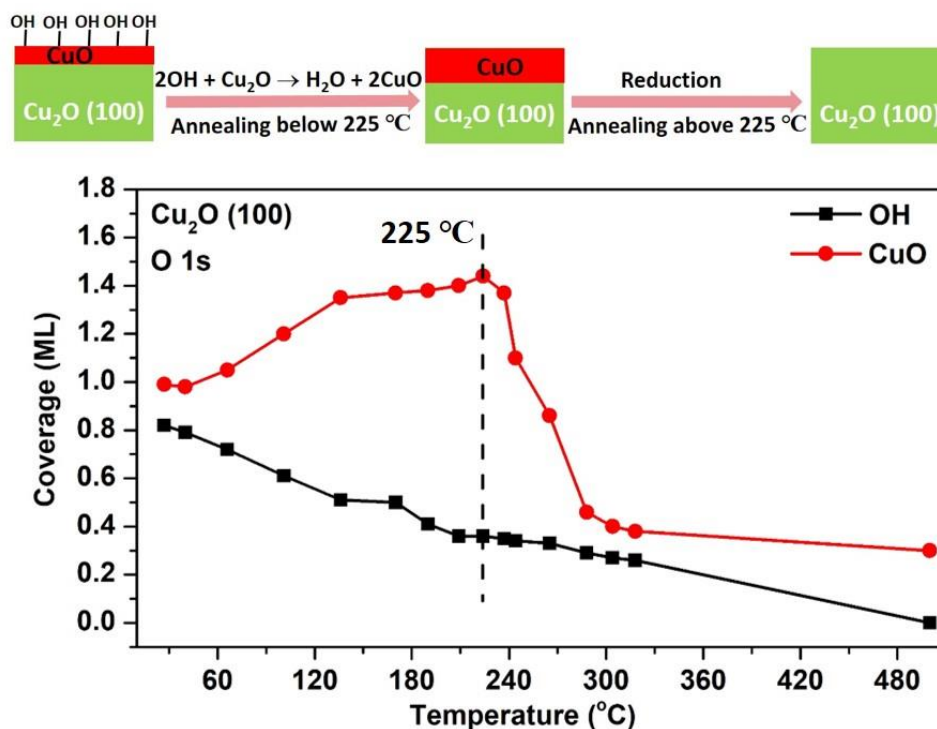
## **6. Acknowledgements**

This work was funded by the Swedish Research Council (VR) and the Knut och Alice Wallenbergs stiftelse. The Ragnar Holm foundation is acknowledged for a fellowship to Heloise Tissot and the Carl Trygger foundation for a fellowship to Chunlei Wang. The staff at MAX IV and ALBA is gratefully acknowledged for support during the beamtimes.

## **7. Supporting information**

The supporting information includes additional XPS results and analysis as well as complementing STM results.

Table of Contents Figure



## 8. References

- Royer, S.; Duprez, D., Catalytic Oxidation of Carbon Monoxide over Transition Metal Oxides. *Chemcatchem* **2011**, 3 (1), 24-65.
- Huang, T. J.; Tsai, D. H., CO oxidation behavior of copper and copper oxides. *Catal Lett* **2003**, 87 (3-4), 173-178.
- White, B.; Yin, M.; Hall, A.; Le, D.; Stolbov, S.; Rahman, T.; Turro, N.; O'Brien, S., Complete CO oxidation over Cu<sub>2</sub>O nanoparticles supported on silica gel. *Nano Lett* **2006**, 6 (9), 2095-2098.
- Baber, A. E.; Yang, X. F.; Kim, H. Y.; Mudiyansele, K.; Soldemo, M.; Weissenrieder, J.; Senanayake, S. D.; Al-Mahboob, A.; Sadowski, J. T.; Evans, J.; Rodriguez, J. A.; Liu, P.; Hoffmann, F. M.; Chen, J. G. G.; Stacchiola, D. J., Stabilization of Catalytically Active Cu plus Surface Sites on Titanium-Copper Mixed-Oxide Films\*\*. *Angew Chem Int Edit* **2014**, 53 (21), 5336-5340.
- Zhang, Z. H.; Wang, S. S.; Song, R.; Cao, T.; Luo, L. F.; Chen, X. Y.; Gao, Y. X.; Lu, J. Q.; Li, W. X.; Huang, W. X., The most active Cu facet for low-temperature water gas shift reaction. *Nat Commun* **2017**, 8.
- Vissokov, G. P., Plasma-chemical preparation of nanostructured catalysts for low-temperature steam conversion of carbon monoxide: properties of catalysts. *Catal Today* **2004**, 89 (1-2), 213-221.
- Hua, Q.; Cao, T.; Gu, X. K.; Lu, J. Q.; Jiang, Z. Q.; Pan, X. R.; Luo, L. F.; Li, W. X.; Huang, W. X., Crystal-Plane-Controlled Selectivity of Cu<sub>2</sub>O Catalysts in Propylene Oxidation with Molecular Oxygen. *Angew Chem Int Edit* **2014**, 53 (19), 4856-4861.
- Schulz, K. H.; Cox, D. F., Propene Oxidation over Cu<sub>2</sub>O Single-Crystal Surfaces - a Surface Science Study of Propene Activation at 1-Atm and 300-K. *J Catal* **1993**, 143 (2), 464-480.
- Tonner, S. P.; Trimm, D. L.; Wainwright, M. S.; Cant, N. W., Dehydrogenation of Methanol to Methyl Formate over Copper-Catalysts. *Ind Eng Chem Prod Rd* **1984**, 23 (3), 384-388.

10. Besharat, Z.; Halldin Stenlid, J.; Soldemo, M.; Marks, K.; Önsten, A.; Johnson, M.; Öström, H.; Weissenrieder, J.; Brinck, T.; Göthelid, M., Dehydrogenation of methanol on Cu<sub>2</sub>O (100) and (111). *The Journal of chemical physics* **2017**, *146* (24), 244702.
11. Centi, G.; Perathoner, S., Nature of Active Species in Copper-Based Catalysts and Their Chemistry of Transformation of Nitrogen-Oxides. *Appl Catal a-Gen* **1995**, *132* (2), 179-259.
12. Paracchino, A.; Laporte, V.; Sivula, K.; Gratzel, M.; Thimsen, E., Highly active oxide photocathode for photoelectrochemical water reduction. *Nat Mater* **2011**, *10* (6), 456-461.
13. Ikeda, S.; Takata, T.; Komoda, M.; Hara, M.; Kondo, J. N.; Domen, K.; Tanaka, A.; Hosono, H.; Kawazoe, H., Mechano-catalysis - a novel method for overall water splitting. *Phys Chem Chem Phys* **1999**, *1* (18), 4485-4491.
14. Auer, E.; Freund, A.; Pietsch, J.; Tacke, T., Carbons as supports for industrial precious metal catalysts. *Applied Catalysis A: General* **1998**, *173* (2), 259-271.
15. Bashyam, R.; Zelenay, P., A class of non-precious metal composite catalysts for fuel cells. *Nature* **2006**, *443* (7107), 63-66.
16. Jaouen, F.; Proietti, E.; Lefèvre, M.; Chenitz, R.; Dodelet, J.-P.; Wu, G.; Chung, H. T.; Johnston, C. M.; Zelenay, P., Recent advances in non-precious metal catalysis for oxygen-reduction reaction in polymer electrolyte fuel cells. *Energy & Environmental Science* **2011**, *4* (1), 114-130.
17. Emsley, J., *Nature's building blocks: an AZ guide to the elements*. Oxford University Press: 2011.
18. Mistry, H.; Varela, A. S.; Bonifacio, C. S.; Zegkinoglou, I.; Sinev, I.; Choi, Y.-W.; Kisslinger, K.; Stach, E. A.; Yang, J. C.; Strasser, P., Highly selective plasma-activated copper catalysts for carbon dioxide reduction to ethylene. *Nat Commun* **2016**, *7*.
19. Rosborg, B.; Werme, L., The Swedish nuclear waste program and the long-term corrosion behaviour of copper. *Journal of Nuclear Materials* **2008**, *379* (1), 142-153.
20. Platzman, I.; Brener, R.; Haick, H.; Tannenbaum, R., Oxidation of polycrystalline copper thin films at ambient conditions. *The Journal of Physical Chemistry C* **2008**, *112* (4), 1101-1108.
21. Kleber, C.; Weissenrieder, J.; Schreiner, M.; Leygraf, C., Comparison of the early stages of corrosion of copper and iron investigated by in situ TM-AFM. *Appl. Surf. Sci.* **2002**, *193* (1), 245-253.
22. Goodman, D., Model catalysts: From extended single crystals to supported particles. *Surface Review and Letters* **1995**, *2* (01), 9-24.
23. Goodman, D. W., Single crystals as model catalysts. *Journal of Vacuum Science and Technology* **1982**, *20* (3), 522-526.
24. Schulz, K. H.; Cox, D. F., Photoemission and low-energy-electron-diffraction study of clean and oxygen-dosed Cu<sub>2</sub>O (111) and (100) surfaces. *Physical Review B* **1991**, *43* (2), 1610.
25. Soldemo, M.; Stenlid, J. H.; Besharat, Z.; Ghadami Yazdi, M.; Önsten, A.; Leygraf, C.; Göthelid, M.; Brinck, T.; Weissenrieder, J., The Surface Structure of Cu<sub>2</sub>O (100). *The Journal of Physical Chemistry C* **2016**, *120* (8), 4373-4381.
26. Önsten, A.; Göthelid, M.; Karlsson, U. O., Atomic structure of Cu<sub>2</sub>O (111). *Surface Science* **2009**, *603* (2), 257-264.
27. Önsten, A.; Weissenrieder, J.; Stoltz, D.; Yu, S.; Göthelid, M.; Karlsson, U. O., Role of defects in surface chemistry on Cu<sub>2</sub>O (111). *The Journal of Physical Chemistry C* **2013**, *117* (38), 19357-19364.
28. Deng, X.; Herranz, T.; Weis, C.; Bluhm, H.; Salmeron, M., Adsorption of water on Cu<sub>2</sub>O and Al<sub>2</sub>O<sub>3</sub> thin films. *The Journal of Physical Chemistry C* **2008**, *112* (26), 9668-9672.
29. Cox, D. F.; Schulz, K. H., H<sub>2</sub>O adsorption on Cu<sub>2</sub>O (100). *Surface Science* **1991**, *256* (1-2), 67-76.
30. Deng, X.; Verdager, A.; Herranz, T.; Weis, C.; Bluhm, H.; Salmeron, M., Surface chemistry of Cu in the presence of CO<sub>2</sub> and H<sub>2</sub>O. *Langmuir* **2008**, *24* (17), 9474-9478.
31. Cox, D. F.; Schulz, K. H., Interaction of CO with Cu<sup>+</sup> cations: CO adsorption on Cu<sub>2</sub>O (100). *Surface science* **1991**, *249* (1-3), 138-148.

32. Bredow, T.; Márquez, A. M.; Pacchioni, G., Analysis of electronic contributions to the vibrational frequency of CO/Cu<sub>2</sub>O (111). *Surface science* **1999**, *430* (1), 137-145.
33. Schulz, K. H.; Cox, D. F., Surface hydride formation on a metal oxide surface: the interaction of atomic hydrogen with Cu<sub>2</sub>O (100). *Surface science* **1992**, *278* (1-2), 9-18.
34. Zhang, R.; Liu, H.; Zheng, H.; Ling, L.; Li, Z.; Wang, B., Adsorption and dissociation of O<sub>2</sub> on the Cu<sub>2</sub>O (111) surface: Thermochemistry, reaction barrier. *Applied Surface Science* **2011**, *257* (11), 4787-4794.
35. Poulston, S.; Parlett, P.; Stone, P.; Bowker, M., Surface oxidation and reduction of CuO and Cu<sub>2</sub>O studied using XPS and XAES. *Surface and Interface Analysis* **1996**, *24* (12), 811-820.
36. Casarin, M.; Maccato, C.; Vigato, N.; Vittadini, A., A theoretical study of the H<sub>2</sub>O and H<sub>2</sub>S chemisorption on Cu<sub>2</sub>O (111). *Applied surface science* **1999**, *142* (1), 164-168.
37. Sun, B.-Z.; Chen, W.-K.; Wang, X.; Lu, C.-H., A density functional theory study on the adsorption and dissociation of N<sub>2</sub>O on Cu<sub>2</sub>O (111) surface. *Applied surface science* **2007**, *253* (18), 7501-7505.
38. Jiang, Y.; Adams, J. B.; Sun, D., Benzotriazole adsorption on Cu<sub>2</sub>O (111) surfaces: a first-principles study. *The Journal of Physical Chemistry B* **2004**, *108* (34), 12851-12857.
39. Yu, X.; Zhang, X.; Tian, X.; Wang, S.; Feng, G., Density functional theory calculations on oxygen adsorption on the Cu<sub>2</sub>O surfaces. *Applied Surface Science* **2015**, *324*, 53-60.
40. Le, D.; Stolbov, S.; Rahman, T. S., Reactivity of the Cu<sub>2</sub>O (100) surface: Insights from first principles calculations. *Surface Science* **2009**, *603* (10), 1637-1645.
41. Hultquist, G., Hydrogen evolution in corrosion of copper in pure water. *Corrosion Science* **1986**, *26* (2), 173-177.
42. Hultquist, G.; Graham, M.; Szakalos, P.; Sproule, G.; Rosengren, A.; Gråsjö, L., Hydrogen gas production during corrosion of copper by water. *Corrosion Science* **2011**, *53* (1), 310-319.
43. Gercher, V. A.; Cox, D. F., Water adsorption on stoichiometric and defective SnO<sub>2</sub> (110) surfaces. *Surface science* **1995**, *322* (1-3), 177-184.
44. Bustillo, F.; Roman, E.; De Segovia, J., Adsorption and thermal desorption of H<sub>2</sub>O on TiO<sub>2</sub> (001) at 250 K. *Vacuum* **1989**, *39* (7-8), 659-661.
45. Zhang, R.; Ludviksson, A.; Campbell, C. T., The chemisorption of H<sub>2</sub>O and O<sub>2</sub> on Cu films on ZnO (0001)-O. *Surface science* **1993**, *289* (1-2), 1-9.
46. Clendening, W.; Rodriguez, J.; Campbell, J.; Campbell, C., The chemisorption and coadsorption of water and oxygen on Cs-dosed Cu (110). *Surface Science* **1989**, *216* (3), 429-461.
47. Nygren, M. A.; Pettersson, L. G., H<sub>2</sub>O interaction with the polar Cu<sub>2</sub>O (100) surface: a theoretical study. *The Journal of Physical Chemistry* **1996**, *100* (5), 1874-1878.
48. Stenlid, J.; Soldemo, M.; Johansson, A.; Leygraf, C.; Göthelid, M.; Weissenrieder, J.; Brinck, T., Reactivity at the Cu<sub>2</sub>O (100): Cu-H<sub>2</sub>O interface: a combined DFT and PES study. *Physical Chemistry Chemical Physics* **2016**, *18* (44), 30570-30584.
49. Zhang, R.; Li, J.; Wang, B.; Ling, L., Fundamental studies about the interaction of water with perfect, oxygen-vacancy and pre-covered oxygen Cu<sub>2</sub>O (111) surfaces: Thermochemistry, barrier, product. *Applied Surface Science* **2013**, *279*, 260-271.
50. Pérez-Dieste, V.; Aballe, L.; Ferrer, S.; Nicolàs, J.; Escudero, C.; Milán, A.; Pellegrin, E. In *Near ambient pressure XPS at ALBA*, Journal of Physics: Conference Series, IOP Publishing: 2013; p 072023.
51. Jiang, P.; Prendergast, D.; Borondics, F.; Porsgaard, S.; Giovanetti, L.; Pach, E.; Newberg, J.; Bluhm, H.; Besenbacher, F.; Salmeron, M., Experimental and theoretical investigation of the electronic structure of Cu<sub>2</sub>O and CuO thin films on Cu (110) using x-ray photoelectron and absorption spectroscopy. *The Journal of chemical physics* **2013**, *138* (2), 024704.
52. Petrik, N. G.; Kimmel, G. A., Reaction kinetics of water molecules with oxygen vacancies on rutile TiO<sub>2</sub> (110). *The Journal of Physical Chemistry C* **2015**, *119* (40), 23059-23067.